https://doi.org/10.21122/1029-7448-2021-64-3-219-227

UDC 621.396.6

A Detection System with Spider Web Coil-Based Wireless Charging and an Active Battery Management System*

J. Pokorny[1)], P. Marcon[1)], T. Kriz[1)], J. Janousek[1)]

[1)]Brno University of Technology (Brno, Czech Republic)

Abstract. The article presents a detection system with spider web coil-based wireless charging. Commonly available metal detectors are sold as handheld systems, which enable only progressive, lengthy, time-consuming search. Importantly, a part of the investigated area can thus be easily missed, and the probability that a metal object will not be found increases substantially. This problem, however, is eliminable via the automatic position tracking mode embedded in the solution obtained through our research. The proposed system facilitates using the spider web coil simultaneously for wireless charging and metal detection by pulse induction. The topology of the detector can emit variable pulse lengths, thus allowing the device to detect more types of metal and to adapt itself to the permeability of the soil. The coil has a branch in a relevant part of the winding to reduce undesirable electromagnetic interference during the charging. On the transmitting side of the topology, impedance matching is included to maintain the maximum spatial gap variability. By changing the position of the receiving side, the output voltage changes; therefore, a high efficiency DC/DC converter is employed. The individual battery cells demonstrate different internal resistances, requiring us to apply a new method to balance the cells voltage. The system can be utilized on self-guided vehicles or drones; advantageously, a GPS resending the coordinates to a mesh radio allows for accurate positioning. With the mesh topology, potential cooperation between the multiple systems is possible. The setup utilizes the same coil for wireless power transfer and detection.

Keywords: wireless power transfer, metal detector, power delivery, active battery management system, pulse induction

For citation: Pokorny J., Marcon P., Kriz T., Janousek J. (2021) A Detection System with Spider Web Coil-Based Wireless Charging and an Active Battery Management System. *Energetika. Proc. CIS Higher Educ. Inst. and Power Eng. Assoc.* 64 (3), 219–227. https://doi.org/10.21122/1029-7448-2021-64-3-219-227

Система обнаружения с беспроводной зарядкой на основе катушки с крестовидной перемычкой и активной системой управления аккумулятором

Й. Покорный[1)], П. Маркон[1)], Т. Криз[1)], Й. Яноусек[1)]

[1)]Технологический университет Брно (Брно, Чешская Республика)

Реферат. В статье представлена система обнаружения с беспроводной зарядкой на основе катушки с крестообразной перемычкой. Обычно доступные металлоискатели продаются

Адрес для переписки
Маркон Петр
Технологический университет Брно
ул. Техническая, 3082/12,
61600, г. Брно, Чешская Республика
Тел.: +420 541-146-281
marcon@vutbr.cz

Address for correspondence
Marcon Petr
Brno University of Technology
3082/12, Technicka str.,
61600, Brno, Czech Republic
Tel.: +420 541-146-281
marcon@vutbr.cz

* The preparation of this paper was assisted by the general student development project in progress at Brno University of Technology.

в виде переносных систем, которые позволяют осуществлять только постепенный, длительный и трудоемкий поиск. Важно отметить, что часть исследуемой зоны, таким образом, может быть легко пропущена, и вероятность того, что металлический объект не будет найден, существенно возрастает. Эта проблема устраняется с помощью автоматического режима отслеживания местоположения, встроенного в решение, полученное в результате наших исследований. Предлагаемая система облегчает одновременное использование катушки с крестообразной перемычкой для беспроводной зарядки и обнаружения металла с помощью импульсной индукции. Топология детектора может излучать переменную длину импульсов, что позволяет устройству обнаруживать больше типов металлов и адаптироваться к проницаемости почвы. Катушка имеет ответвление в соответствующей части обмотки, чтобы уменьшить нежелательные электромагнитные помехи во время зарядки. На передающей стороне топологии включено согласование импеданса для поддержания максимальной изменчивости пространственного зазора. При изменении положения приемной стороны изменяется выходное напряжение, поэтому используется высокоэффективный преобразователь постоянного тока в постоянный. Отдельные элементы батареи демонстрируют различные внутренние сопротивления, что требует применения нового метода для балансировки напряжения элементов. Система может быть использована на самонаводящихся транспортных средствах или беспилотных летательных аппаратах; GPS, успешно отправляющие координаты на многоканальное радио, обеспечивают точное позиционирование. При наличии многоканальной топологии возможно потенциальное сотрудничество между разнообразными системами. В установке используется одна и та же катушка для беспроводной передачи и обнаружения энергии.

Ключевые слова: беспроводная передача питания, металлоискатель, подача питания, активная система управления аккумулятором, импульсная индукция

Для цитирования: Система обнаружения с беспроводной зарядкой на основе катушки с крестовидной перемычкой и активной системой управления аккумулятором / Й. Покорный [и др.] // *Энергетика. Изв. высш. учеб. заведений и энерг. объединений СНГ*. 2021. Т. 64, № 3. С. 219–227. https://doi.org/ 10.21122/1029-7448-2021-64-3-219-227

Introduction

Wireless charging has been used for more than a hundred years influencing the development of Tesla transformer. At the present, wireless charging can be used in small electronics to charge electric cars and it is heavily involved in electrical engineering department. There is no use of charging connectors, but the number of components increases. The trend is a resonant or inductive charging. Both methods use different topologies and geometric shapes to transfer the energy. The resonance method carries the possibility of charging up to several tens of centimeters [1, 2], while induction results in higher efficiency and lower interference [3–5].

Pilot's intervention is not necessary as the unmanned aerial vehicle's (UAV) flight path is controlled by the real-time image detection where the variability and a number of various detected waypoints need to be processed. It is possible to perform a completely autonomous flight from take-off of the aircraft to landing [6, 7].

Various speed and altitude may be set during the flight and additional accessories may be controlled by the drone. The use of real-time image detection on an autonomous flight of the UAV can serve for package delivery, mapping of large areas, or for military missions and other security forces [8–12].

System topology

The design of the wireless power transfer and pulse induction detection system consists of transmitting and receiving parts (Fig. 1). The first block of the

transmitting part is a power source for the whole unit. The power source can be realized by an adapter or a power bank that contains standard power delivery and can supply up to 100 W of power. This standard includes the CYPD3135 [13] chip with the CCG3 standard from Cypress which also has a 32-bit ARM processor and can be used as a station monitor.

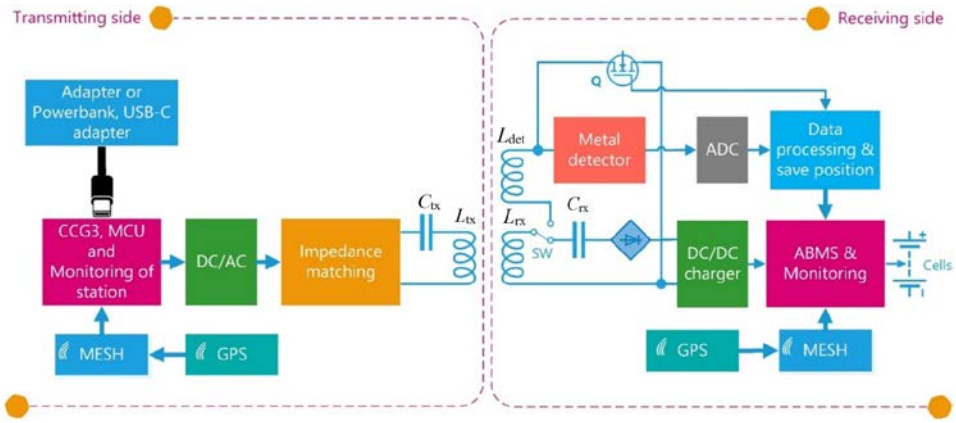

Fig. 1. Topology of the detection and charging system

The chip enables the supply of power to the DC/AC block, which generates an alternating voltage for the serial resonant circuit with transmitting coil L_{tx} and capacitor C_{tx}. The impedance tuning block adjusts the impedance of the transmission resonant circuit L_{tx} and C_{tx} and can improve the transmission efficiency even if the coils are not exactly offset. It also adjusts the mutual inductance M between the coils which is effective by the coupling factor k according to the equation (1) as follows

$$M = k\sqrt{L_{tx}L_{rx}} \ [\mathrm{H}], \tag{1}$$

where L_{rx} – receiving coil.

The mutual inductance in this equation is given only by the coupling factor k, which varies with the distance of the coils and the current consumption of the receiving part. The degree of interaction between the receiving coil L_{rx} and the transmitting coil L_{tx} is a function of the distance and the positional arrangement.

On the receiving side, the coil is realized as a spider web coil with a threaded branch for charging. Part of the coil can be used for charging called L_{rx} or the whole winding $L_{rx} + L_{det}$ can be used for metal detection. The rectifier makes for rectifying the energy. This energy is adjusted to the required voltage to the battery cells by the DC/DC converter. The battery cells are controlled by an active battery management system (ABMS). To suppress the electromagnetic field, an L_{rx} coil with an optimized flowing current according to the charging power is reversed by means of a transistor Q.

For metal detection, the charging system disconnects part of the charging winding L_{rx} and the entire winding L_{det} is used. Then the signal response is processed by the analog-to-digital converter (ADC) part discussed in the next block

diagram, see Fig. 2. The combination of subsequent processing and logging the position saves the data on the charger monitoring. Both parties can have a mesh radio that transmits data to the receiving party. The mesh radio is implemented by the XBEE SX 868 module [14]. The structure of the output data frames depends on the transmission mode. Received data together with coordinates from the navigation module (GPS) can be forwarded to the transmitting party. Then, it is stored via the universal asynchronous receiver-transmitter or serial peripheral interface on a storage device and it can send the coordinates of the detected targets.

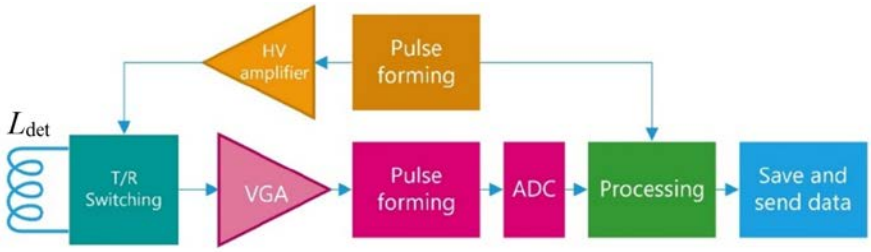

Fig. 2. Block diagram of metal detector

Pulse induction detector topology

The basic topology of the pulse induction metal detector in Fig. 3 is detected by the L_{det} detection coil using formed pulses from the HV 7361 module [15]. The module implements T/R switching with a voltage pulse height of ±100 V at the current of 2.5 A with the possibility of operating frequency up to 35 MHz. The module also has adjustable switch between reception and transmission using the input logic gates that shape the pulse.

To adjust the received pulse, the AD8331 variable gain amplifier is used for pulse detection and guarantees a dynamic range throughout the amplifying the signal up to 48 dB due to the programmable gain and input resistance setting [16]. The ADL5511 pulse detector [17] can send an envelope of received signal or RMS voltage to the transmitter. Then the signal is further sampled by the ADC 10-bit AD9200 [18] converter with a maximum sampling frequency of 20 Msps. For a conventional embedded system, signal processing is sufficient for the conventional metal detection. For experiments with more complex processing and visualization of more complex structures, it is necessary to use an array of programmable gate arrays. The processed data can be stored on a storage device or sent by the mesh radio together with the coordinates using the ISM band only if an important object is detected or can be sent permanently.

Design of spider web coil

The spider web coil was widely used in older radio receivers on the long waves up to very short waves (λ = 2000 m to 1 m). Wireless charging works on the similar frequencies. The advantage of this coil is its small parasitic capacity due to the method of winding. Another advantage is the high inductance

achieved by the presence of a large surface area by which it can receive or transmit. The coil design is based on the Archimedean spiral, where the mass point rotates around the *z*-axis into three-dimensional space at an angular velocity ω and starts from the point at time *t* [19]. The position of the point relative to the *z*-axis is then as follows:

$$\begin{aligned} v_x &= v\cos(\omega t) - \omega(vt + c)\sin(\omega t); \\ v_y &= v\sin(\omega t) + \omega(vt + c)\cos(\omega t), \end{aligned} \tag{2}$$

where $(vt + c)$ – modulus of the position vector of the mass point at time *t*, from which the velocity components v_x and v_y for the *x* and *y* axes are derived.

If we integrate the given equations (2) in parts, their parametric expression are as follows:

$$\begin{aligned} x &= (vt + c)\cos(\omega t); \\ y &= (vt + c)\sin(\omega t), \end{aligned} \tag{3}$$

where the point at time *t* must change sinusoidally.

The coil model is plotted in Fig. 3.

a b

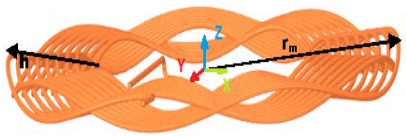


```
close all;
r = 100; %outer radius
a = 70;    %inner radius
b = 1; %incerement per rev % Jos: changed to see the spiral!!
n = (r - a)./(b); %number  of revolutions
th = 2*n*pi;     %angle
Th = linspace(0,th,n*360);
x = (a + b.*Th/(2*pi)).*cos(Th);
y = (a + b.*Th/(2*pi)).*sin(Th);
angle = linspace(0,2*pi,360)
z = 10*cos(9*Th/2); % -----------------
```

Fig. 3. Spider web coil: a – coil design according to equations (3); b – script for MatLab

Active battery management

It is beneficial to choose ABMS due to the tolerances in the internal resistance or temperature conditions of individual batteries. If an undervoltage occurs on one cell, the balancer disconnects the battery from the load. The advantages of the topology are simplicity and complexity at the expense of the size of the hardware design.

A pair of MOSFETs of Fig. 4 switching the coil is used. The pair is charged from the lower cell for a time given by the inductance of the coil and the voltage of the $Cell_{low}$ cell according to (4)

$$\delta t = L\frac{\delta I}{\delta U}\ [\mathrm{s}], \tag{4}$$

where the length of the MOSFET switching time δt is given by the influence of inductance *L* and the inductive energy given by the voltage difference δU and

current difference δ*I*. This time is crucial for not exceeding the maximum cell voltage.

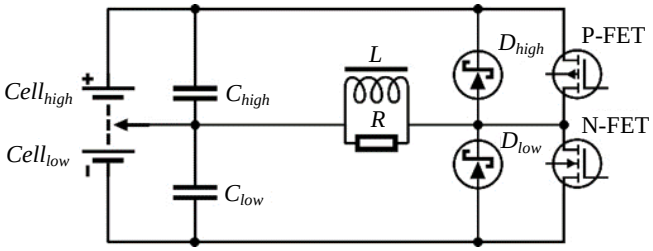

Fig. 4. Balancing between individual cells

During this time, the N-FET must be turned on. In the next cycle, the coil is discharged into the $Cell_{high}$ cell via a parallel D_{high} diode. The same principle can be used for charging a $Cell_{low}$ cell from a P-FET. The gates of the transistors can be controlled by a controller or a PWM regulator according to the voltage of individual cells, but mostly by the capacity of the accumulators, from which the size of the inductor and the length of switching are derived.

Simulations

The theoretical inductance is compared with the actual inductance in Tabl. 1. As expected, the coils of these values have large tolerance (usually 20 %). Theoretical values of the multiple threads differ. The first factor is winding of the threads, and the second factor is neglecting of the supply wires. The coil will have different properties for different frequencies.

Table 1

Comparison of measured and calculated values for the spider web coil

Wire diameter	0.65 mm
Inner radius	120 mm
Outer radius	156 mm
Number of turns for charging	6
Calculated inductance for charging	8.4 µH
Measured inductance for charging (10 kHz)	10.1 µH
DC resistance	0.1 Ω
Number of turns for detection	26
Calculated inductance for detection	184.22 µH
Measured inductance for charging (10 kHz)	154.8 µH
DC resistance	0.73 Ω

With the entered parameters, the simulation was performed for a step change in voltage (Fig. 5a). There is 1, 5, 10 and 30 µs of the pulse lengths in the simulation. Fig. 5 visualizes the responses of the coil oscillation due to its parasitic capacity. R_1 forms the series of the winding resistance and C_1 the parasitic capacitance. According to equation (5), the induced voltage on the coil is given by the pulse size of the source V_1, the ratio of the resistor divider R_1 and R_2, and the exponential function of the negative pulse t length divided by the transient state of the coil τ

$$u_L(t) = L\frac{\delta i_L}{\delta t} = -V_1\frac{R_1 + R_2}{R_2}e^{\frac{-t}{\tau}}. \quad (5)$$

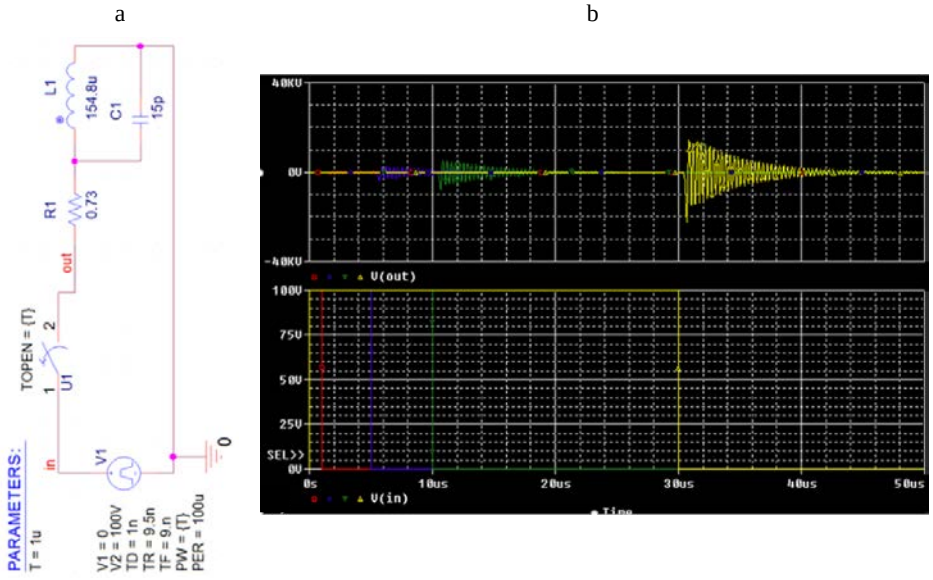

Fig. 5. Coil response without discharge resistance for pulse lengths 1, 5, 10 and 30 µs: a – connection of the coil to the pulse source; b – voltage peak when opening switch U_1

By adding the resistor R_2 in the diagram in Fig. 6a, which simulates the input impedance of the HV7360 module [14], the parasitic capacitance of capacitor C_1 to R_2 is not applied and the voltage peak is induced due to the very fast current dissipation by the coil L_1. The exact value can be determined accordingly to the equation (5), where τ is the time constant.

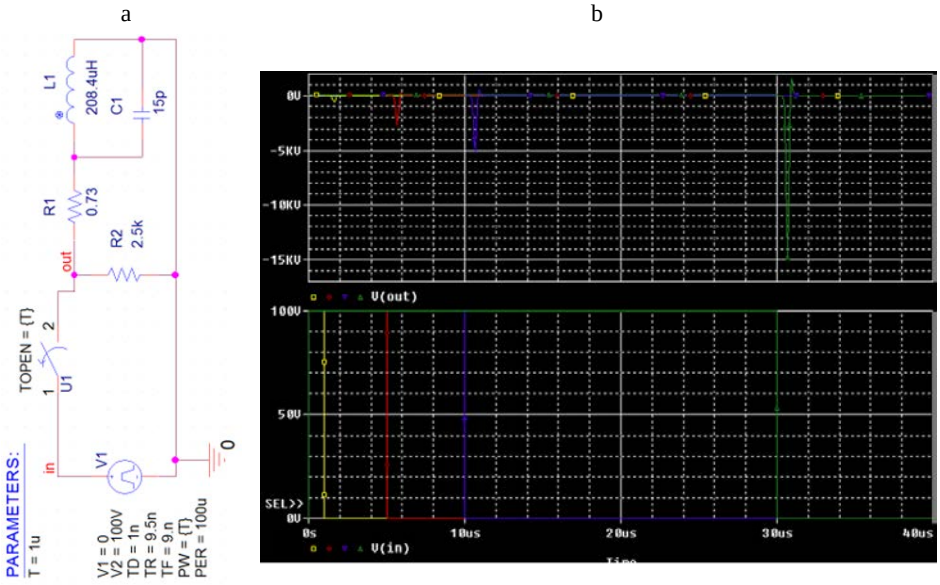

Fig. 6. Coil response with discharge resistance for pulse lengths 1, 5, 10 and 30 µs: a – adding impedance; b – overvoltage peak on the coil without oscillations

Simulation for recharging the cell

For a Li-Ion cell with a capacity of 2500 mAh with a nominal voltage of 3.7 V, the switching time for charging an inductor of 15 µH is equal by the equation (4). Equation (6) provides a calculation of the switching time of transistors δt for a specified Li-Ion cell

$$\delta t = L\frac{\delta I}{\delta U_{Cell_{high}}} = 15\cdot 10^{-6}\frac{2.5}{3.7} = 10.13\ \mu s. \tag{6}$$

The discharge time in equation (7) is slightly shorter due to the higher voltage drop across the Schottky diode. To improve power transfer efficiency, the power MOSFET is in parallel with an open Schottky diode on at 8.92 µs

$$\delta t = L\frac{\delta I}{\delta\left(U_{Cell_{high}} + U_{D_{high}}\right)} = 15\cdot 10^{-6}\frac{2.5}{3.7+0.5} = 8.92\ \mu s. \tag{7}$$

For given calculation, the scheme from Fig. 4 in P-spice was performed followed by the time analysis for the course of the voltage on the $Cell_{high}$. In the connection, the cells represent resistors R_5 and R_6 because the ideal batteries hold a constant voltage; thereby, it represents an ideal voltage source. The pulse source has parameters according to equation (4). The bottom graph in Fig. 7 shows the voltage peak from 95 mV coil as a result of the mean value of the voltage on the $Cell_{high}$ increases by 220 µV and periodizes at 160 µV from 150 µs until the balancing stops and the $Cell_{high}$ voltage is equal to $Cell_{low}$.

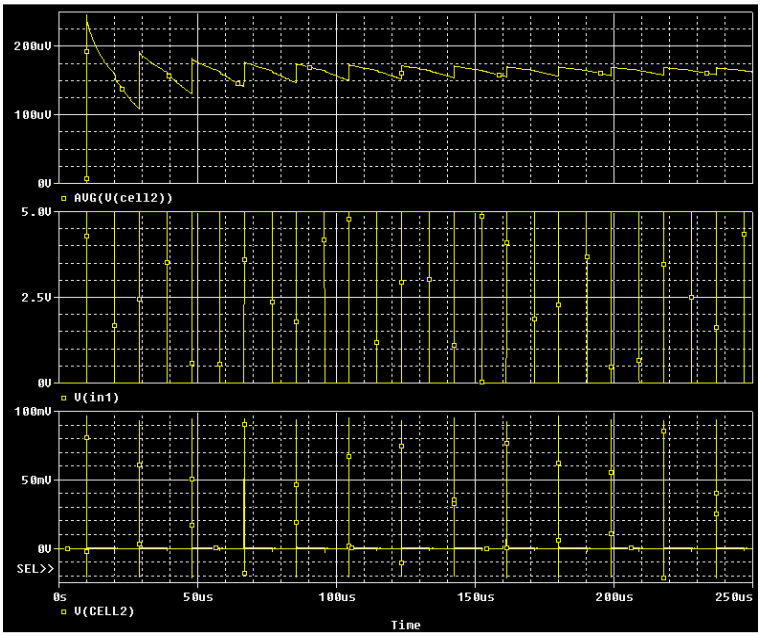

Fig. 7. Voltage increase on $Cell_{high}$ at switching time t = 10 µs of N-FET transistor

CONCLUSION

The article describes a proposed topology that allows wireless charging without the need for the precise centering due to the fine tuning with the use of

the impedance matching which is not addressed in this article. The proposed charging via the USB-C connector allows charging with the use of standardized adapters or power banks. A coil winding like spider web coil also allows the detection of various objects according to the settings and processing of the amount of pulse energy. The active balancing system makes it possible to transfer the energy between adjacent cells in the event of different internal resistance and thus use their full capacity. Advantageously, it can be used for an autonomous system for easy charging and detection of metal objects.

REFERENCES

1. Valtchev S., Valtchev S. (2019) Control for the Contactless Series Resonant Energy Converter. *Emerging Capabilities and Applications of Wireless Power Transfer,* 102–140. https://doi.org/10.4018/978-1-5225-5870-5.ch005.
2. Valtchev S., Medeiros R., Valtchev S., Klaassens B. (2011) An Instantaneous Regulation for the Wired and Wireless Super-Resonant Converters. *IEEE 33rd International Telecommunications Energy Conference (INTELEC),* 1–8. https://doi.org/10.1109/intlec.2011.6099875.
3. Gigov G., Krusteva A., Valtchev S. (2016) Experimental Study of Wireless Inductive System for Electric Vehicles Batteries Charging. *IEEE International Power Electronics and Motion Control Conference (PEMC),* 290. https://doi.org/10.1109/epepemc.2016.7752012.
4. *Electronics World* (1920). New York: Ziff-Davis Publishing Company. 998.
5. Mahmood M. F., Mohammed S. L., Gharghan S. K., Al-Naji A., Chahl J. (2020) Hybrid Coils-Based Wireless Power Transfer for Intelligent Sensors. *Sensors,* 20 (9), 2549. https://doi.org/10.3390/s20092549.
6. Gabrlik P., Jelinek A., Janata P. (2016) Precise Multi-Sensor Georeferencing System for Micro UAVs. *IFAC-PapersOnLine,* 49 (25), 170–175. https://doi.org/10.1016/j.ifacol.2016.12.029.
7. Gabrlik P. (2015) The Use of Direct Georeferencing in Aerial Photogrammetry with Micro UAV. *IFAC-PapersOnLine,* 48 (4), 380–385. https://doi.org/10.1016/j.ifacol.2015.07.064.
8. Janousek J., Marcon P., Pokorny J., Mikulka J. (2019) Detection and Tracking of Moving UAVs. *Photonics & Electromagnetics Research Symposium – Spring (PIERS-Spring),* 2759–2763. https://doi.org/10.1109/piers-spring46901.2019.9017351.
9. Pokorny J., Marcon P., Janousek J., Kriz T., Dohnal P. (2019) A Wireless Charging Station for Multipurpose Electronic Systems. *Photonics & Electromagnetics Research Symposium – Spring (PIERS-Spring),* 2093–2097. https://doi.org/10.1109/piers-spring46901.2019.9017278.
10. Grechikhin L. I., Saharuk D. A., Sivashko A. B., Tsanava A. A. (2010) Energy of Unmanned Aerial Vehicle (UAV) Windmill (Theory, Streamlined Airflow). *Energetika. Izvestiya Vysshikh Uchebnykh Zavedenii i Energeticheskikh Ob'edinenii SNG = Energetika. Proceedings of the CIS Higher Education Institutions and Power Engineering Associations,* (4), 59–68 (in Russian).
11. Lukovnikov V. I., Rudchenko Y. A., Samovendyuk N. V. (2011) Determination of Small Parameter of Auto-Oscillating "Single-Phase Asynchronous Motor – Linear Elastic Element System". *Energetika. Izvestiya Vysshikh Uchebnykh Zavedenii i Energeticheskikh Ob'edinenii SNG = Energetika. Proceedings of the CIS Higher Education Institutions and Power Engineering Associations,* (3), 5–9 (in Russian).
12. Dedek J., Golembiovsky M., Slanina Z. (2017) Sensoric System for Navigation of Swarm Robotics Platform. *18th International Carpathian Control Conference (ICCC),* 429–433. https://doi.org/10.1109/carpathiancc.2017.7970438.
13. *EZ-PD™ CCG3, USB Type-C Port Controller.* Available at: https://www.cypress.com/file/222281/download.
14. *Digi XBEE SX 868 Modul.* Available at: https://www.digi.com/products/embedded-systems/digi-xbee/rf-modules/sub-1-ghz-rf-modules/digi-xbee-sx-868.
15. *High-Speed ±100V 2.5A Two-or-Three-Level Ultrasound Pulsers*. Available at: http://ww1.microchip.com/downloads/en/DeviceDoc/20005570A.pdf.
16. *Ultralow Noise VGAs with Preamplifier and Programmable RIN.* Available at: https://manualzz.com/doc/7930643/ultralow-noise-vgas-with-preamplifier-and-programmable-r---.
17. *Complete 10-Bit, 20 MSPS, 80 mW CMOS A/D Converter.* Available at: https://manualzz.com/doc/13384652/a-complete-10-bit--20-msps--80-mw-cmos-a-d-converter-ad9200.
18. *DC to 6 GHz Envelope and TruPwr RMS Detector*. Available at: https://www.analog.com/media/en/technical-documentation/data-sheets/ADL5511.pdf.
19. Line Mathematics. *Britannica.* Available at: https://www.britannica.com/science/line-mathematics.

Received: 21 October 2020 Accepted: 18 February 2021 Published online: 31 May 2021